JOURNAL OF GEOPHYSICAL RESEARCH, VOL. 106, NO. A10, PAGES 21,525–21,541, OCTOBER 1, 2001

Observations of persistent Leonid meteor trails 2. Photometry and numerical modeling

C. A. Kruschwitz[1], M. C. Kelley[1], C. S. Gardner[2], G. Swenson[2], A. Z. Liu[2], X. Chu[2], J. D. Drummond[3], B. W. Grime[3], W. T. Armstrong[4], J. M. C. Plane[5], and P. Jenniskens[6]

Abstract. During the 1998 Leonid meteor shower, multi-instrument observations of persistent meteor trains were made from the Starfire Optical Range on Kirtland Air Force Base, New Mexico, and from a secondary site in nearby Placitas, New Mexico. The University of Illinois Na resonance lidar measured the Na density and temperature in the trains, while various cameras captured images and videos of the trains, some of which were observed to persist for more than 30 min. The Na density measurements allow the contribution of Na airglow to the observed train luminescence to be quantified for the first time. To do this, persistent train luminescence is numerically modeled. Cylindrical symmetry is assumed, and observed values of the Na density, temperature, and diffusivity are used. It is found that the expected Na luminosity is consistent with narrowband CCD all-sky camera observations, but that these emissions can contribute only a small fraction of the total light observed in a 0.5-1 μ bandwidth. Other potential luminosity sources are examined, in particular, light resulting from the possible excitation of monoxides of meteoric metals (particularly FeO) and $O_2(b^1\Sigma_g^+)$ during reactions between atmospheric oxygen species and meteoric metals. It is found that the total luminosity of these combined processes falls somewhat short of explaining the observed brightness, and thus additional luminosity sources still are needed. In addition, the brightness distribution, the so-called hollow cylinder effect, remains unexplained.

1. Introduction

One of the most fascinating and puzzling of meteoric phenomena is that of persistent meteor trains, self-luminous clouds that linger for several minutes after the passage of a meteor. A typical meteor train fades very quickly, lasting for only a few seconds, but a persistent train can endure for up to an hour or even longer. Such trains are extremely rare, occurring only as a result of bright meteors, and are typically associated with high-velocity meteor showers such as the Leonids or the Perseids. The first recorded observations of persistent trains date back over 100 years to those of *Newton* [1869], and they have been the subject of substantial investigation since. However, an explanation for the sustained luminescence of the trains remains elusive.

Perhaps the most widely accepted explanation for persistent train luminescence was put forth by *Chapman* [1955]. He suggested that the oxidation by O_3 of neutral Na atoms deposited by the meteoroid during its ablation in the atmosphere and the subsequent reduction of the resulting NaO by atmospheric O could lead to excited Na atoms, which could then radiate. This is the same mechanism responsible for the Na airglow. The complete Na oxidation-reduction sequence is

$$\mathrm{Na} + \mathrm{O_3} \longrightarrow \mathrm{NaO} + \mathrm{O_2}, \quad (1)$$

$$\mathrm{Na} + \mathrm{O_2} + \mathrm{N_2} \longrightarrow \mathrm{NaO_2} + \mathrm{N_2}, \quad (2)$$

$$\mathrm{NaO_2} + \mathrm{O} \longrightarrow \mathrm{NaO} + \mathrm{O_2}, \quad (3)$$

$$\mathrm{NaO} + \mathrm{O_3} \longrightarrow \mathrm{NaO_2} + \mathrm{O_2} \longrightarrow \mathrm{Na} + 2\mathrm{O_2}, \quad (4)$$

$$\mathrm{NaO} + \mathrm{O} \longrightarrow \mathrm{Na}(^2\mathrm{P}) + \mathrm{O_2} \longrightarrow \mathrm{Na}(^2\mathrm{S}) + \mathrm{O_2}, \quad (5)$$

[1]School of Electrical and Computer Engineering, Cornell University, Ithaca, New York.
[2]Department of Electrical and Computer Engineering, University of Illinois, Urbana, Illinois.
[3]Starfire Optical Range, Directed Energy Directorate, Air Force Research Laboratory, Kirtland Air Force Base, Albuquerque, New Mexico.
[4]Los Alamos National Laboratory, Los Alamos, New Mexico.
[5]School of Environmental Sciences, University of East Anglia, Norwich, England, United Kingdom.
[6]Search For Extraterrestrial Intelligence Institute, NASA Ames Research Center, Moffet Field, California.

Paper number 2000JA000174.
0148-0227/01/2000JA000174$09.00

Table 1. Reaction Rates for Na Cycle

Reaction			Rate	
$Na + O_3$	$\longrightarrow$	$NaO + O_2$	$k_1 = 1.05 \times 10^{-9} \exp[-116/T]$	$cm^3\ s^{-1}$
$Na + O_2 + N_2$	$\longrightarrow$	$NaO_2 + N_2$	$k_2 = 5.0 \times 10^{-30}[T/200]^{-1.22}$	$cm^6\ s^{-1}$
$NaO_2 + O$	$\longrightarrow$	$NaO + O_2$	$k_3 = 5.0 \times 10^{-10} \exp[-940/T]$	$cm^3\ s^{-1}$
$NaO + O_3$	$\longrightarrow$	$NaO_2 + O_2$	$k_{4a} = 1.11 \times 10^{-9} \exp[-568/T]$	$cm^3\ s^{-1}$
	$\longrightarrow$	$Na + 2O_2$	$k_{4b} = 3.2 \times 10^{-10} \exp[-550/T]$	$cm^3\ s^{-1}$
$NaO + O$	$\longrightarrow$	$Na(^2P) + O_2$	$k_5 = 2.2 \times 10^{-10}[T/220]^{1/2}$	$cm^3\ s^{-1}$
	$\longrightarrow$	$Na(^2S) + O_2$		

$$Na(^2P) \longrightarrow Na(^2S) + h\nu, \quad (6)$$

where photons emitted in (6) have a wavelength of 589 nm, the well-known Na D lines. The rates for these reactions have been measured [*Plane and Helmer*, 1994] and are presented in Table 1. However, the branching ratio α, which indicates how much of the Na created in (5) is created in the ^2P state, is poorly known, with estimates ranging from 0.01 to 0.6. A value of 0.1 will be used for α here consistent with the laboratory results of *Clemesha et al.* [1995], though recent results from the Sudden Atom Layer (SAL) rocket flight indicate a much lower value of around 0.02 for α [*Hecht et al.*, 2000]. *Baggaley* [1975] closely investigated the feasibility of the Na oxidation-reduction cycle as a possible source of train luminosity. At that time the rates of the reactions were not well known, and consequently, the early results were less than promising: even using a value of 1.0 for α, Baggaley found that a meteor of visual magnitude -10.75 or brighter would be required to produce Na emissions of sufficient intensity to be visible to the naked eye. Later work, using improved rate coefficient estimates [*Baggaley*, 1978; *Kolb and Elgin*, 1976], found the Na cycle to be capable of producing as much as 10^3 times more luminosity than Baggaley had originally shown, lowering the limit to -3.25 magnitude, which is in agreement with observations.

Until now, it was unclear if, indeed, all visual luminosity arose from this mechanism. Experimental evidence supporting the *Chapman* [1955] mechanism has been lacking because of the scarcity of persistent train spectral information. Because persistent trains are both rare and unpredictable, good spectral measurements are difficult to obtain. A few spectra, however, do exist. Persistent train spectra have been reported by *Borovička et al.* [1996], *Rajchl et al.* [1995], and *Abe et al.* [2001]. In particular, the *Abe et al.* [2001] train was that of a Leonid fireball during the 1998 shower. Strong Na emissions at the 589 nm wavelength are a feature common to all of these spectra, providing support for the *Chapman* [1955] theory. However, strong emissions from other meteoric metals, particularly Mg and Fe, are also detected, as are emissions from metal oxides.

More recent Leonid storm observations from the Leonid Multi-Instrument Aircraft campaign now show that many of these emissions are a feature of secondary ablation [*Borovička and Jenniskens*, 2000]. All prior spectra were captured relatively early in the life of the train and thus may not reflect the spectrum of the train after it has developed for some time. Indeed, visible spectra obtained minutes after train formation are lacking many of these lines. Rather, a broad continuum is observed that has been identified with FeO "orange arc" emission [*Jenniskens et al.*, 2000b], underlaying the sodium emission lines. FeO emission is a product of the *Chapman* [1955] airglow mechanism involving meteoric iron.

Near-IR emissions from a persistent train have also been detected by broadband imaging techniques [*Hapgood*, 1980]. Using a low-light television camera, Hapgood detected strong emissions between 700 and 900 nm from the persistent train of a -6 absolute magnitude meteor. While these emissions cannot be due to Na or FeO, Hapgood speculated that they may yet be due to the *Chapman* [1955] cycle. He suggested that radiation resulting from the excitation of the O_2, formed in (5), into its $b^1\Sigma_g^+$ state and the subsequent transition to the $X^3\Sigma_g^-$ ground state could be the source of the emissions. Unfortunately, whether or not (5) produces a significant amount of $O_2(b^1\Sigma_g^+)$ has never been verified, although it is sufficiently exothermic to do so provided $Na(^2P)$ is not produced. Given that the branching ratio α is predicted to be small, it seems possible that there may be a large amount of $O_2(b^1\Sigma_g^+)$ produced in (5).

This paper is a second in a series describing the observations of those trains [see *Drummond et al.*, this issue]. In this paper, the feasibility of the *Chapman* [1955] Na cycle as a source of enduring meteor train luminosity is revisited in the light of new observations made of several persistent trains during the 1998 Leonid meteor shower. A numerical model of a meteor train similar to that described by *Baggaley* [1975] and *Kolb and Elgin* [1976] is used to calculate the expected Na emissions. This basic model is then expanded to include possible

$O_2(b^1\Sigma)$ emissions resulting from Na chemistry, as well as from metals and metal oxides expected to be present in large quantities, namely, Fe, Ca, and Mg.

Further clues to the luminosity mechanism are found from the peculiar dynamical properties of the persistent trains. In particular, we investigate the "hollow" appearance many trains exhibit, as reported by *Newton* [1869] and many other observers since [*Trowbridge*, 1911; *Hawkins*, 1957]. Under sufficient magnification, such a train appears as two parallel trains separated by a region of darkness. This peculiar feature was thought by *Trowbridge* [1911] to be due to the train's having the shape of a hollow cylinder, with radiation from the outer rim of the cylinder far exceeding that from the region closer to its axis, an explanation that has gained wide support. A definitive explanation for the central depletion, however, has not yet been put forth. *Baggaley* [1976] suggested that charge exchange between neutral Na atoms and meteoric metal ions could lead to a large depletion of Na atoms, which would, in turn, lead to a depletion in luminosity. Since, according to this model, the density of metal ions is much greater toward the axis of the train, the depletion will be far more pronounced there. An alternative explanation has been discussed by *Kelley et al.* [2000], *Chu et al.* [2000], and *Jenniskens et al.* [2000c]. They suggest that the depletion of O_3 as a result of (1) of the *Chapman* [1955] cycle may be significant enough at the train's center, where the density of Na and other metals is greatest, to lead to appreciably less luminosity being produced there relative to the train's outer regions. The numerical model developed in this paper is used to examine this hypothesis in greater detail.

In our study, we will address available measurements of sodium by lidar and narrowband imaging techniques and visible spectroscopic measurements of persistent trains obtained during the 1998 and 1999 Leonid showers. During the peak of the 1998 Leonid meteor shower on November 17 the first ever resonance lidar observations of persistent meteor trains were made from the Starfire Optical Range (SOR), a facility of the Air Force Research Laboratory, Directed Energy Directorate, on Kirtland Air Force Base near Albuquerque, New Mexico. SOR is home to a 3.5 m steerable optical telescope, which has been adapted for use as a Na resonance lidar by the University of Illinois. The capabilities of the lidar are such that Na temperature and the mesospheric winds can be measured in addition to the Na density. The fact that the telescope is steerable makes it ideal for use in the study of persistent trains, which endure long enough to allow the lidar beam to be guided to them. Once the lidar detects the Na enhancement left by the meteor, the train can be tracked by following the enhancement, even after the train's emissions have grown too faint to be seen by either the naked eye or the image-intensified cameras used in the experiment. In this way, measurements were made of seven persistent trains, three of which were tracked on the order of 30 min. Further details of the experiment are reported by *Drummond et al.* [this issue]. Preliminary reports on the 1998 Leonid campaign at SOR have been published by *Kelley et al.* [2000], *Grime et al.* [2000], *Chu et al.* [2000], and *Drummond et al.* [2000]. These results are complemented by spectroscopic measurements of persistent trains onboard the Leonid Multi-Instrument Aircraft Campaign, a two-aircraft mission to the Mediterranean, during the 1999 Leonid storm of November 18. The mission is described by *Jenniskens et al.* [2000a]. One train was observed with a slit-based visible spectrograph, while another was observed with a slitless spectrograph, both minutes after the fireball.

2. Observations

Plate 1 shows images of three of the seven persistent trains observed at SOR on November 17. Brief details of each are given below; further information is given by *Kelley et al.* [2000], *Grime et al.* [2000], *Chu et al.* [2000], and *Drummond et al.* [2000, this issue].

The train shown in Plate 1a will be of primary interest in this paper because it is for this train that we have the most comprehensive set of measurements. Dubbed "Diamond Ring" because of its ring-like appearance, this train resulted from a meteor that occurred at 0927:50 UT. Two visual observers estimated a brightness of -1.5 (absolute magnitude -2), but similar estimates for the meteor that caused another persistent train (the "Rope") and that was observed by intensified video cameras to be of apparent visual magnitude -6.6±0.6 suggest that the brightness of the Diamond Ring meteor was about -8 magnitude. A single image of high spatial resolution was obtained that enables accurate photometry. This image was taken with a CCD camera with a 2° field of view 82 s after the initial appearance of the meteor. At that time the train was still visible to the naked eye, and it continued to be visible for ~3 min more. The bandwidth of the CCD camera is approximately from 0.5 to 1 μ, and hence the camera would have detected Na *D* line emissions, FeO and other metal oxide emissions, and any infrared emissions of the type reported by *Hapgood* [1980], which he attributed to $O_2(b^1\Sigma)$. The dual appearance of the "ring" portion of the train is an ideal illustration of the hollow effect alluded to earlier and will be discussed in greater detail in section 5.

The train shown in the CCD image in Plate 1b, called the "Glowworm", was by far the most visually spectacular of all the trains observed during the SOR Leonid campaign. It was the result of a -14.3 magnitude meteor [*Zinn et al.*, 1999] (Note, SOR visual observers estimated <-4.5 magnitude), the brightest seen that night, and was still clearly visible to the naked eye more than 10 min after its initial appearance at 1005:44 UT. Unfortunately, because of its location in the sky, no lidar

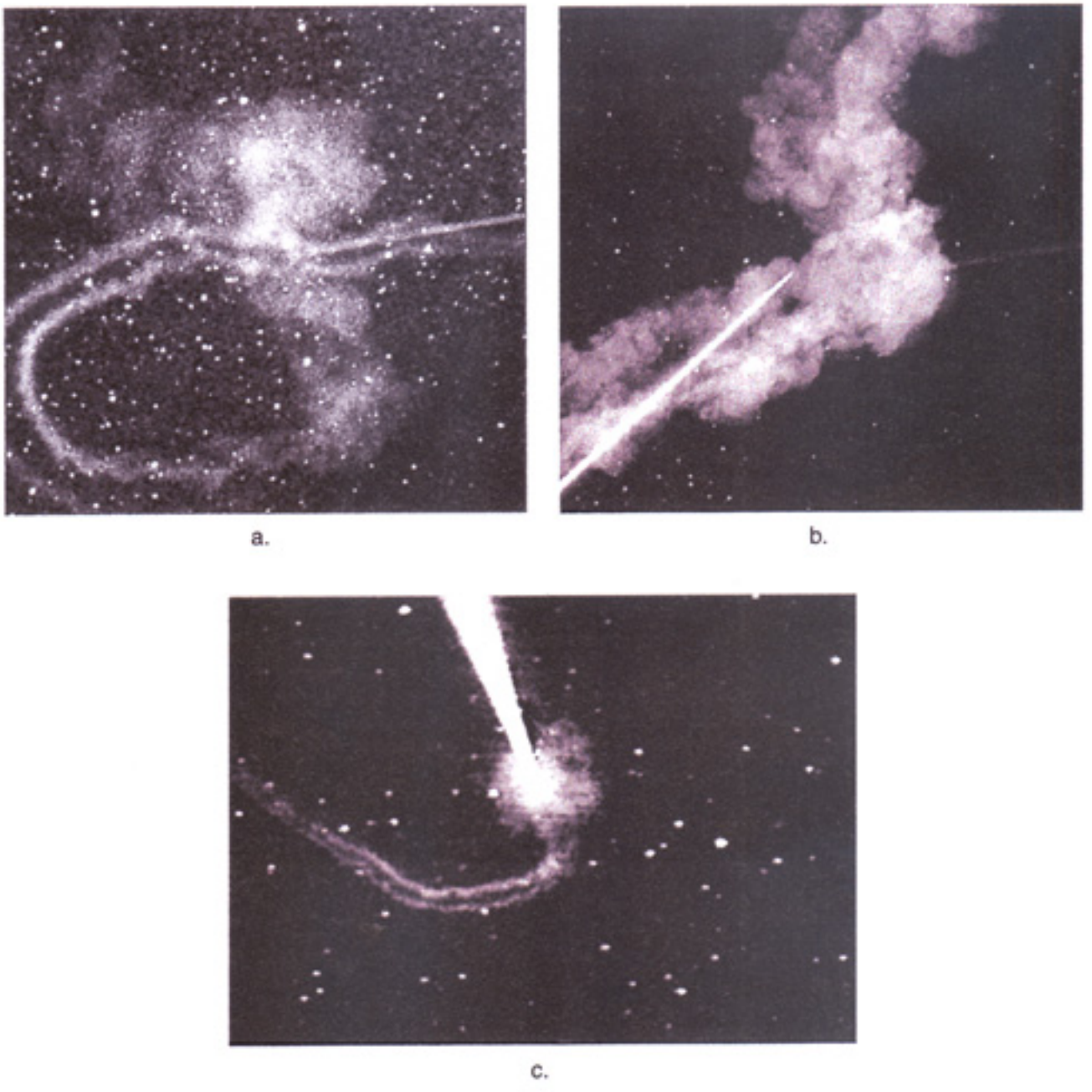

Plate 1. Images of several persistent trains being probed by lasers from the SOR on November 17, 1998. Reproduced from *Kelley et al.* [2000].

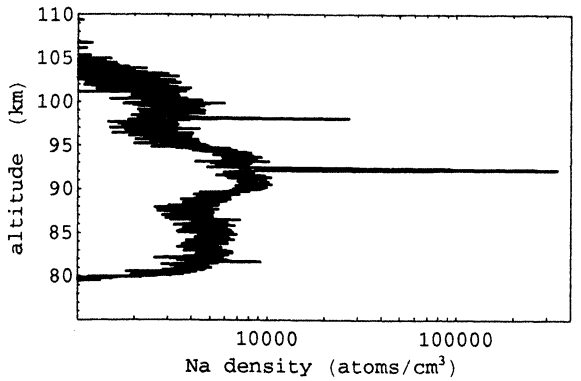

Figure 1. Na Resonance lidar profile from the Diamond Ring meteor trail. Reproduced from *Chu et al.* [2000].

data could be obtained for this train, but an all-sky camera was able to track Na 589 nm emissions from the train for more than an hour [*Kelley et al.*, 2000].

The train in Plate 1c is another excellent example of a hollow train. This train is referred to as the "Straightened Diamond Ring" because of its similarity in appearance to the Diamond Ring, particularly in the resemblance of the "puff" at the end of the former to the "diamond" portion of the latter. The image is a screen capture from a Xybion image-intensified video camera with a 5° field of view that was attached to the headring of 3.5 m telescope. The bright line coming from the top of the image is the Na laser. This train resulted from a meteor that occurred at 0951:42 UT and remained visible for about 5 min. The lidar was able to track it for ~11 min [*Chu et al.*, 2000].

A Na profile from the Diamond Ring obtained shortly after the lidar located its Na enhancement, about 1 min after the initial meteor, is shown in Figure 1. The typical background sodium layer of about 5000 atoms cm^3 is clearly evident in the profile. The dual Na spikes are a result of the lidar beam intersecting the trail at two altitudes, 92.5 and 98 km. The enhancement at 98 km was tracked for nearly half an hour. The peak Na densities measured for this trail were 3.41×10^5 and 1.95×10^5 cm^{-3} for the lower and upper trail portions, respectively [*Chu et al.*, 2000]. The Na atom line density q has also been calculated. This is defined as

$$q = 2n_{\text{peak}}\pi\sigma^2, \tag{7}$$

where n_{peak} is the peak Na number density and σ is taken from fitting a Gaussian $A\exp(-x^2/2\sigma^2)$ to the meteor's Na trail and correcting for the angle θ between the lidar beam and the trail. Values for q ranged from about 2.0×10^{13} cm^{-1} to about 1.5×10^{14} cm^{-1}. Figure 2 shows a series of lidar profiles for the lower Diamond Ring Na enhancement. Of the eight profiles shown, four show some sign of a second smaller peak in addition to the main peak, but there is no evidence of an appreciable depletion in the Na density. This would seem to argue against the Baggaley charge exchange mechanism as a viable process for producing the *Trowbridge* [1911] hollow cylinder of luminosity. The gradual decrease in height of the enhancement is not to be interpreted as a fall speed; since the train is distributed over a large range of heights, what appears to be the trail falling to lower altitudes is likely the lidar intercepting lower-altitude portions of the trail.

In addition to the Na resonance lidar, two all-sky cameras were used to observe the trains. One of these, operating at SOR, was fixed with a 750-900 nm band-

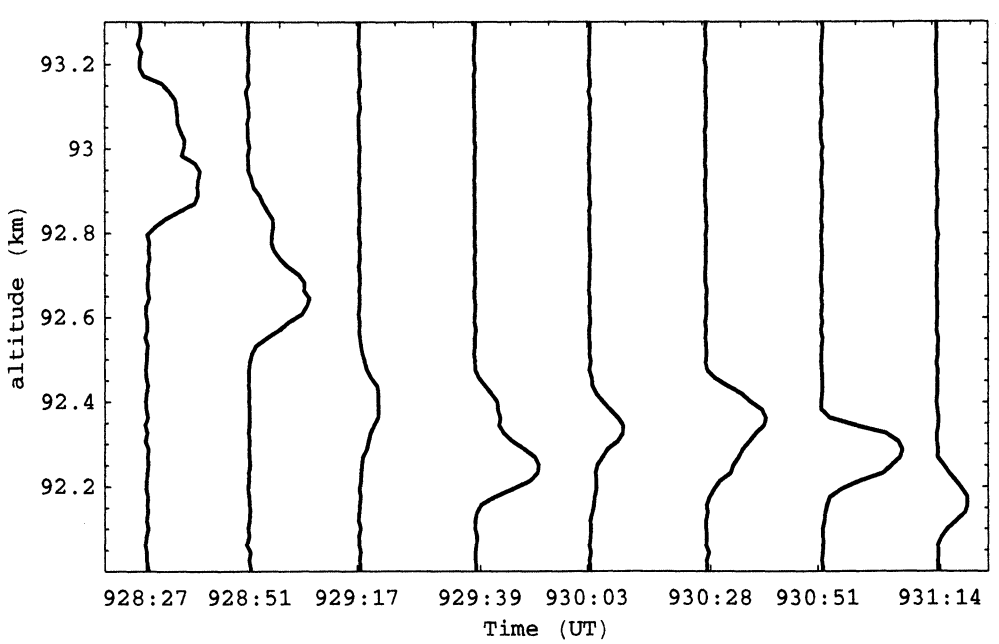

Figure 2. Series of Na resonance lidar profiles from the lower Na enhancement of the *Diamond Ring*.

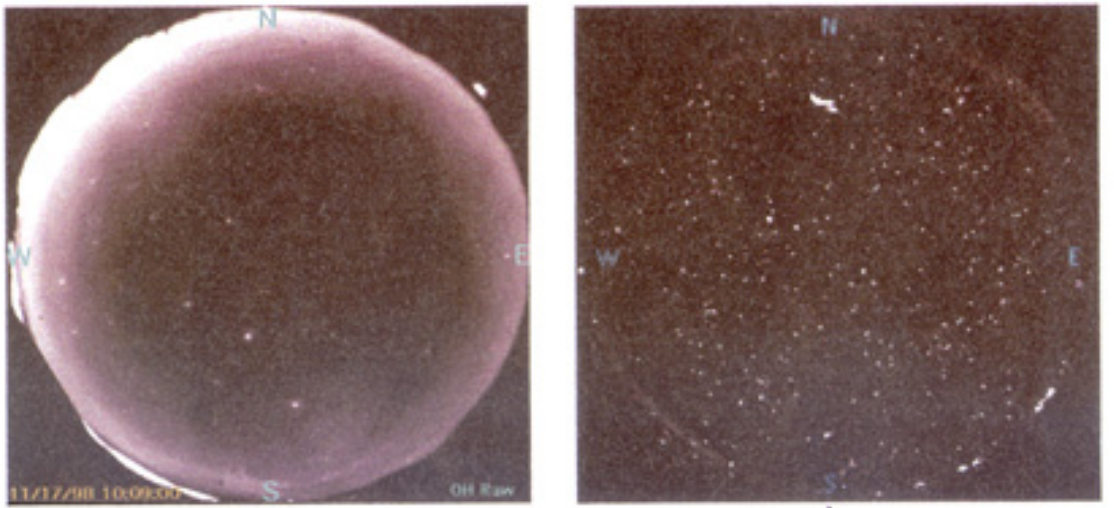

Plate 2. All-sky images of the Glowworm. (a) OH image, taken from SOR. The emissions persisted for just over 20 min. (b) Na image, taken from Placitas, New Mexico, about 40 km North of SOR. The 589 nm emissions persisted for over an hour.

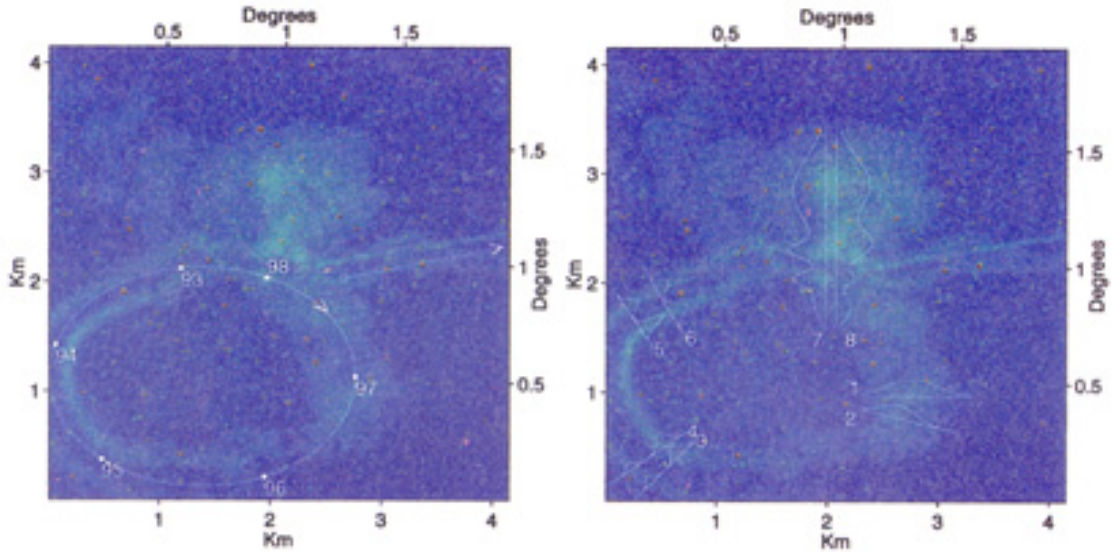

Plate 3. (left) The theoretical trajectory of the Diamond Ring parent meteor and the loop part of the trail 82 s later. Altitudes are shown at various points along the loop portion of the trail. The hollow circles along the theoretical trajectory indicate altitudes of 98 and 97 km. (right) The location of cuts across the trail with the fitted intensity profiles displayed along the cuts.

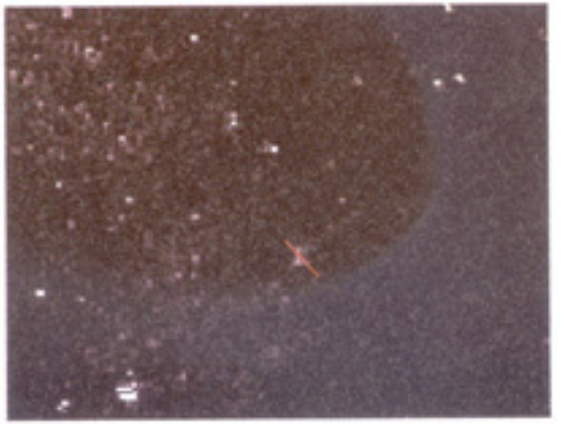

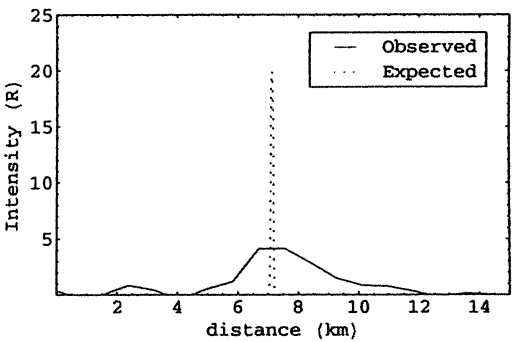

Plate 4. (top) Image from the narrowband Na all-sky imager of the Diamond Ring. (bottom) Expected Diamond Ring Na emissions based on model calculations (narrow peak), and measured background-subtracted Na emissions along line shown in Plate 4(top), assuming a background Na emission of 50 R.

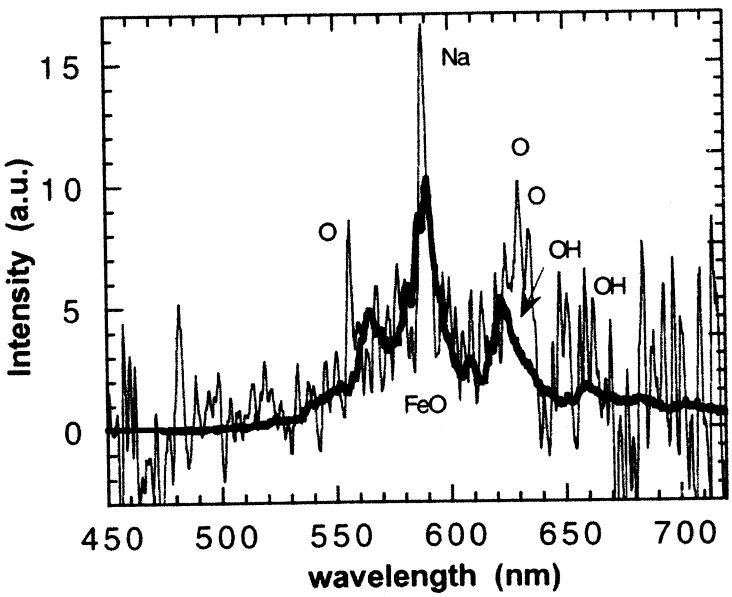

Figure 3. Spectrum of a persistent meteor train obtained during the 1999 Leonid shower. Superimposed is an FeO orange system spectrum. Reproduced from: *Jenniskens et al.* [2000c].

width filter, notched at around 868 nm to block $O_2(b^1\Sigma \rightarrow X^3\Sigma)(0,1)$ atmospheric emissions. This camera is used to observe OH airglow, but it detected emissions from the brightest of the trains observed that night, the Glowworm, for more than 20 min. An image of the Glowworm taken by this camera is shown in Plate 2a.

The second all-sky camera used during the 1998 observations was fixed with a narrowband Na (589 nm) filter and placed at a nearby site in Placitas, New Mexico, about 40 km north of SOR. This camera detected long-lasting emissions from 10 meteor trains, 7 of which correspond to trains also observed at SOR. Na emissions from most of the trains were seen for up to 30 min, but the Glowworm produced detectable Na emissions for well over an hour [*Kelley et al.*, 2000]. A Na image of the Glowworm is shown in Plate 2b. Typical peak intensities measured by the camera were on the order of 100 R above the background Na layer emissions but were found to range from as weak as a few R to as strong as 600 R above the background. Such emissions, though substantial, are still well below the minimum intensity detectable by the human eye. Nevertheless, the presence of Na airglow emissions from the trains was proved, leaving open the question of what fraction of the total luminosity of the trains could be explained by Na emissions and just how the trains could be as bright as indicated by the quantitative results presented next.

Other than these narrowband observations, we have no further spectroscopic information for these events. However, spectra from a persistent train were obtained by *Jenniskens et al.* [2000b] during the 1999 Leonid shower and are reproduced in Figure 3. The strong Na line is evident, as is a broad emission between 530 and 630 nm. This is thought to be due to excited states of the metal oxide FeO. A similar broad emission was observed in the slitless spectrum of a particularly bright -13 magnitude fireball at 0400:29 UT by *Borovička and Jenniskens* [2000]. The slitless spectrum shows no apparent sodium signal because of the much lower spectral resolution. Residual oxygen and what may be OH emission in the spectrum by *Jenniskens et al.* [2000b] remain unexplained and are thought to be residuals from variations in the background airglow. Note that the spectrum does not extend far enough to include the near IR O_2 bands reported by *Hapgood* [1980].

3. Analysis of Photometric Observations

A CCD camera attached to a 400 mm lens was used for our quantitative study. Images of the Diamond Ring, one of the more spectacular trains observed during the 1998 Leonid, are shown in Plate 3. The image shows a loop in the trail, which analysis indicates could be caused by an internal gravity wave with an intrinsic period of 19.5 hours, a horizontal wavelength of 2650 km, and a vertical wavelength of 5.5 km [*Drummond et al.*, this issue]. These values are comparable to results from trimethyl aluminum (TMA) releases and other lidar observations.

Four stars identified in the field of the Diamond Ring image were used to calibrate the CCD camera, which enabled flux measurements at cuts across the trail. These measurements are the first of their kind and, as will be discussed later, point to the inadequacy of current models of persistent trains. Starting with the flux density f (photons m^{-2} s^{-1}), derived from counts at the detector, the surface brightness of each pixel can be calculated by dividing by the pixel area:

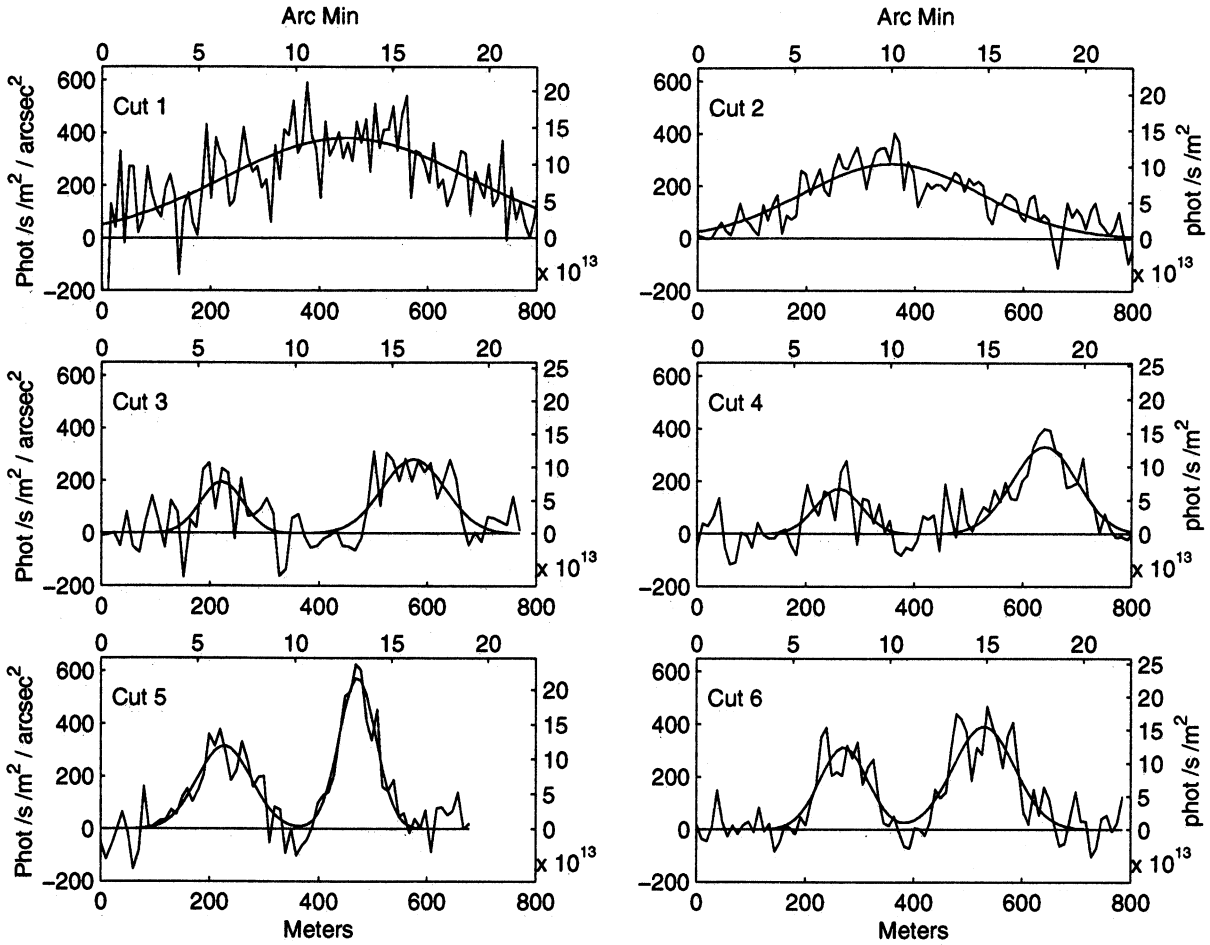

Figure 4. Surface brightness from cuts 1-6 across the ring of the trail. The cuts are fit as one Gaussian or two independent Gaussians, plus a local background, which is subtracted. The scale on the right axis shows surface emission rates.

$$\mathrm{sb} = f/(13.91'')^2 \text{ photons s}^{-1}\text{ m}^{-2}\text{ arcsec}^{-2}. \quad (8)$$

The cuts were then fit with Gaussians:

$$\mathrm{sb} = A\exp(-x^2/2\sigma^2). \quad (9)$$

Using cylindrical geometry, let the z axis be along the trail, which makes an angle of θ with the line of sight the y axis, and let the x axis be normal to the cylinder in the plane of the sky. The surface emission rate at the source, se, can be found by multiplying the surface brightness equation (8) by $4\pi d\sin\theta$ and converting the square arc seconds in (9) to square meters at the source, where d, the distance to the trail, and θ are known because the trajectory of the original meteor is known [*Drummond et al.*, this issue]. The surface emission at the source is given by

$$\begin{aligned}\mathrm{se} &= 4\pi d^2\sin\theta\,\mathrm{sb}\frac{13.91^2}{l^2} \\ &= 4\pi d^2\sin\theta\frac{13.91^2}{l^2}A\exp(-x^2/2\sigma^2) \\ &\qquad \text{photons m}^{-2}\text{ s}^{-1}, \quad (10)\end{aligned}$$

where l is the length of a pixel in meters. Figure 4 shows both the surface brightness and the surface emission across cuts 1-6, while Figure 5 shows the surface brightness for cuts 7 and 8. Figure 6 shows not only the surface brightness for cuts 1-6 as a function of height but two lidar profiles as well. The various parameters for each cut are given in Table 2. For cuts 7 and 8 through the brightest diamond portion of the image the area is confused and covers the region of overlap. Therefore we list the average distance of 122.6 km, the average pixel size of 8.27 m, and a θ of 50° in Table 2. We note that since the light arises from two different parts of the path at different altitudes, the surface brightness or derived line emissions should probably be divided in half for cuts 7 and 8 to give values for one of the contributing paths.

Integrating the surface emission all the way across the trail yields the total line emission rate in all directions from the source as a function of distance along the trail. Because the fits are Gaussians, the total integrated line emission $\mathrm{le_t}$ is

$$\begin{aligned}\mathrm{le_t} &= 4\pi d^2\sin\theta\frac{13.91^2}{l^2}A\sqrt{2\pi}\,\sigma \\ &\qquad \text{photons m}^{-1}\text{ s}^{-1}, \quad (11)\end{aligned}$$

where A and σ are the Gaussian fit parameters listed

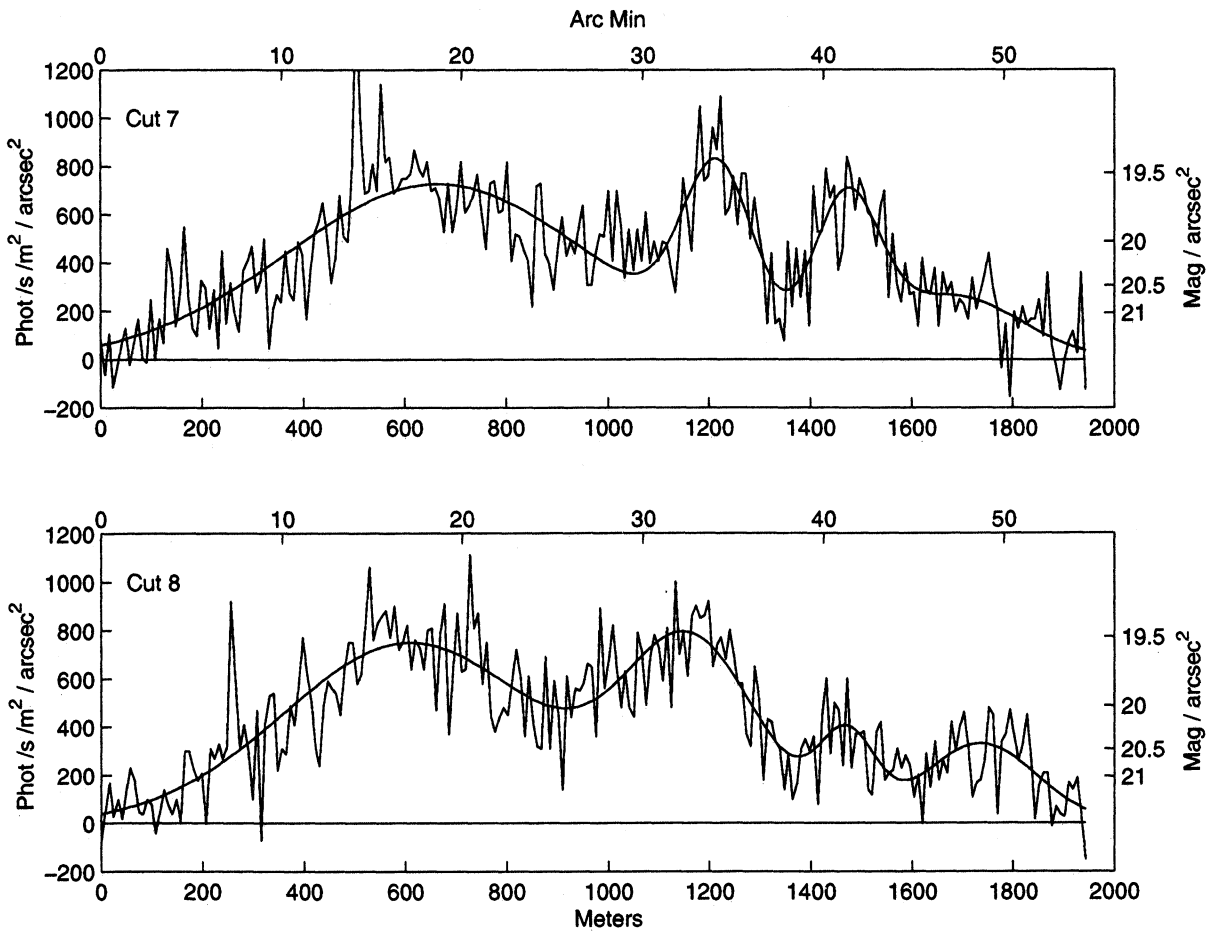

Figure 5. Surface brightness from cuts 7 and 8 across the Diamond Ring. The fits are done as four independent Gaussians, plus a local background which is subtracted. The right axis scale shows brightness in astronomical magnitudes.

in Table 2 and l is the pixel length appropriate for the cut. The total calculated line emission for each cut is given in Table 2 for cuts 1-6. They are not given for 7 and 8 because the region is confused, and no attempt was made to make the cut at right angles to the trail as was done for cuts 1-6. The uncertainty assigned to le_t includes the uncertainty in the Gaussian fit amplitudes and σs, as well as a 10% uncertainty in the blackbody calibration of counts to flux density. These photometry measurements will be compared to the modeling results that follow.

Before moving on to describe the modeling efforts, though, it is interesting to compare the calibrated intensity measurements of the Diamond Ring to those given by *Hapgood* [1980] for the meteor he observed. As mentioned above, he detected the persistent train of a -6 absolute magnitude non-Leonid meteor using a camera with a passband of 700-900 nm and found a photon flux of 2×10^8 photons m^{-2} s^{-1}. (We recalculate the blackbody flux density and find that the fifth magnitude A0 star used to calibrate his camera should produce 5.5×10^7 photons m^{-2} s^{-1}, one third Hapgood's value. In the following the corrected values are included in square brackets.) This translates to a line emission rate of 2×10^{17} [6.2×10^{16}] photons m^{-1} s^{-1}, compared to the average total emission rate for cuts 1-6 of $4.0 \pm 0.5 \times 10^{16}$ photons m^{-1} s^{-1}. Clearly, the intensity of the emissions for the trains is comparable. This is consistent with the Diamond Ring meteor magnitude of around -8 inferred from the video. If the magnitude was closer to the -2 visual estimate, however, then the Diamond Ring train would have been far brighter compared to Hapgood's train than would be expected, perhaps indicating that the train was far brighter in the 500-700 nm and 0.9-1 μ spectral regions not visible to Hapgood's camera.

4. Comparison to Emission Calculations

The numerical model described here is similar to that used by *Baggaley* [1975] and *Kolb and Elgin* [1976]. It models the diffusion and chemical kinetics of a meteor trail, assuming the trail to be a cylindrically symmetric distribution of ablated atoms. A Na atom line density of 1×10^{14} cm^{-1} is used, which is within the range of line densities calculated for the Diamond Ring. This value is consistent with not only the Diamond Ring but most of the other trains observed as well, most of which

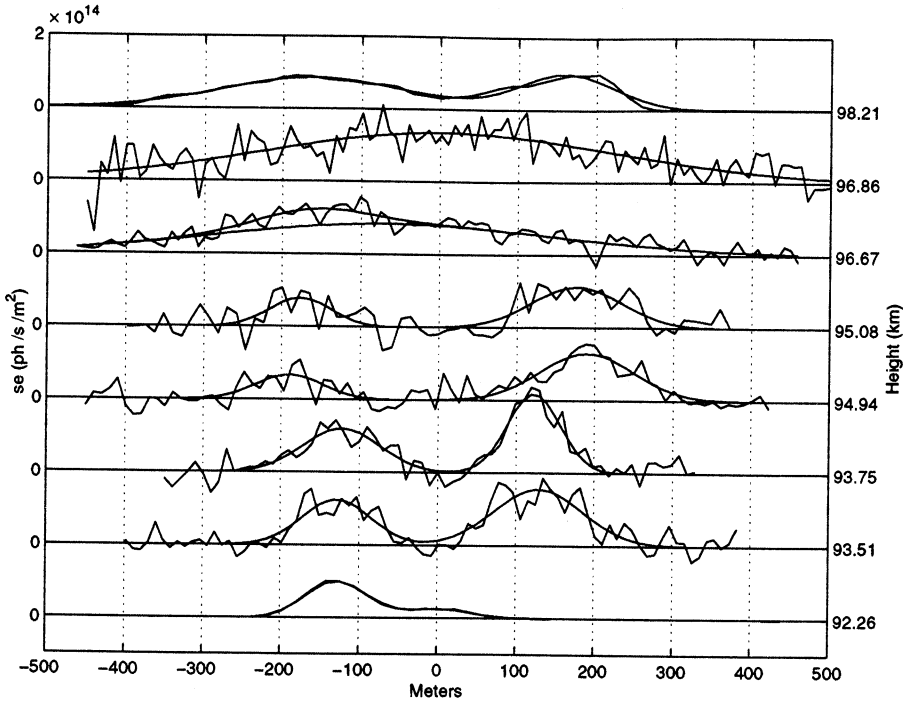

Figure 6. Surface emission rates as a function of altitude. The double structure begins to appear at an altitude of about 96.5 km. The top and bottom curves are Gaussian fits to the lidar data, shown with arbitrary maxima and corrected for the angle between the lidar beam and the trail. The curve at 96.67 km is not the same as in Figure 4 for cut 2, but shows instead that a single Gaussian underlies a broader fog.

were from meteors of a similar size and brightness. The radial profile of this distribution is taken to be Gaussian, and an initial radius of 1 m is used. From this initial size the trail is allowed to evolve under the influence of diffusion, while the ablated Na reacts with atmospheric species via the Chapman cycle of (1)-(5) at the rates given in Table 1. The evolution of the trail is described by the following equations:

$$\frac{\partial}{\partial t}[\mathrm{Na}] = D\nabla^2[\mathrm{Na}] - k_1[\mathrm{Na}][\mathrm{O_3}] + k_{4b}[\mathrm{NaO}][\mathrm{O_3}] - k_2[\mathrm{Na}][\mathrm{O_2}], \quad (12)$$

$$\frac{\partial}{\partial t}[\mathrm{NaO}] = D\nabla^2[\mathrm{NaO}] - k_5[\mathrm{NaO}][\mathrm{O}] + k_1[\mathrm{Na}][\mathrm{O_3}] + k_3[\mathrm{NaO_2}][\mathrm{O}] - (k_{4a} + k_{4b})[\mathrm{NaO}][\mathrm{O_3}], \quad (13)$$

$$\frac{\partial}{\partial t}[\mathrm{NaO_2}] = D\nabla^2[\mathrm{NaO_2}] - k_3[\mathrm{NaO_2}][\mathrm{O}] + k_{4a}[\mathrm{NaO}][\mathrm{O_3}] + k_2[\mathrm{Na}][\mathrm{O_2}][\mathrm{N_2}], \quad (14)$$

$$\frac{\partial}{\partial t}[\mathrm{O_3}] = D\nabla^2[\mathrm{O_3}] - k_1[\mathrm{Na}][\mathrm{O_3}] - (k_{4a} + k_{4b})[\mathrm{NaO}][\mathrm{O_3}], \quad (15)$$

$$\frac{\partial}{\partial t}[\mathrm{O_2}] = D\nabla^2[\mathrm{O_2}] + k_5[NaO][O] + k_1[Na][O_3] + k_3[\mathrm{NaO_2}][\mathrm{O}] + (k_{4a} + 2k_{4b})[\mathrm{NaO}][\mathrm{O_3}] - k_2[\mathrm{Na}][\mathrm{O_2}][\mathrm{N_2}], \quad (16)$$

$$\frac{\partial}{\partial t}[\mathrm{O}] = D\nabla^2[\mathrm{O}] - k_5[\mathrm{NaO}][\mathrm{O}] - k_3[\mathrm{NaO_2}][\mathrm{O}], \quad (17)$$

where D is the diffusivity and the brackets indicate number densities. A value of $D = 5$ m^2 s^{-1} is used here, in agreement with the values calculated by *Grime et al.* [2000] using the lidar data and a simple diffusion estimate. The values reported there ranged from 5 ± 2 to 10 ± 5 m^2 s^{-1}, consistent with molecular diffusion at mesospheric heights. Although these trails are below the turbopause, eddy diffusion does not seem to operate at these scales. Similar conclusions have come from the analysis of TMA trails (M. Larsen, private communication, 2000). Since the chemical reaction rates are temperature-dependent, a temperature of 180 K is used, also typical of the observed trails [*Grime et al.*, 2000]. The number densities of background species used are appropriate for the atmosphere at about 95 km: $[\mathrm{O_3}] = 1.0 \times 10^8$ cm^{-3}, $[\mathrm{O_2}] = 8.0 \times 10^{12}$ cm^{-3}, $[\mathrm{N_2}] = 3 \times 10^{13}$ cm^{-3}, and $[\mathrm{O}] = 5.0 \times 10^{11}$ cm^{-3}. These values were obtained us-

Table 2. Gaussian Fit Parameters

	Amplitude, photons $m^{-2}s^{-1}$ arcsec^{-2}	Center, m	σ, m	Height, km	d, km	θ, deg	l m pix^{-1}	$le_t \times 10^{16}$, photons s^{-1} m^{-1}
1	380±49	450±15	224±37	96.86	124.1	42	8.3703	7.62±1.77
2	283±17	356±8	163±13	96.67	123.9	43	8.3582	4.23±0.60
3	197±47	221±13	39±19	95.08	123.6	48	8.3361	0.77±0.42
	283±50	574±9	58±13					1.64 ± 0.49
Total								2.41±0.65
4	172±28	260±9	42±11	94.94	123.5	47	8.3334	0.71±0.23
	333±22	640±5	59±7					1.93 ± 0.32
Total								2.64±0.40
5	316±30	226±5	49±6	93.75	122.1	45	8.2379	1.47±0.27
	576±34	472±2	34±3					1.86 ± 0.26
Total								3.33±0.37
6	312±33	270±5	44±5	93.51	121.6	48	8.2034	1.35±0.26
	391±28	527±5	57±5					2.20 ± 0.34
Total								3.55±0.43
7	727±77	666±14	298±36	95.25	122.6	50	8.2732	
	699±58	1219±7	70±8					
	613±155	1472±11	65±13					
	261±86	1683±76	134±80					
8	750±61	610±15	253±28	95.25	122.6	50	8.2732	
	723±51	1163±12	129±12					
	342±65	1472±13	56±14					
	331±72	1737±18	111±28					

ing the thermosphere/ionosphere/mesosphere(TIME)-GCM atmospheric model and are provided courtesy of R. Roble.

A finite difference scheme is used to solve (12)-(17) at subsequent time steps for the species abundance at several radial points. The photon emission rate resulting from (6) is then calculated using the following formula:

$$I = k_5[\mathrm{NaO}][\mathrm{O}]\alpha,$$

where I has units of photons cm^3 s^{-1}. Figure 7 shows the Na D line volume emission rate as a function of radial distance for the model trail after it has evolved for 82 s, the same amount of time the Diamond Ring had evolved before the image in Plate 3 was taken. Clearly the emissions are not most intense at the center of the trail as might be expected but at some distance from its axis. This is due to the depletion of ozone in the central regions of the trail where the concentration of Na is greatest and hence where more O_3 is destroyed by the Chapman cycle. This is precisely the effect predicted by *Kelley et al.* [2000], *Chu et al.* [2000], and *Jenniskens et al.* [2000c] to cause the hollow appearance of the train in Plate 1a.

To assess the validity of the numerical results, the expected Na emissions are compared to the results

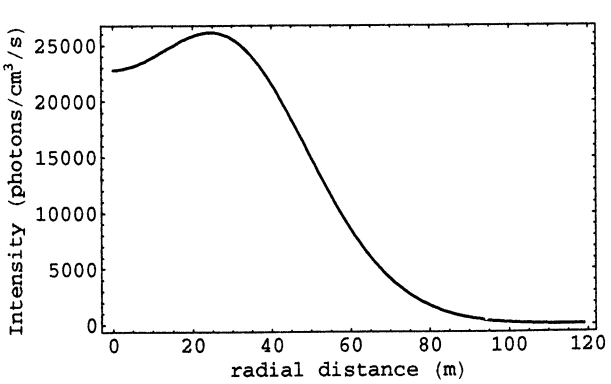

Figure 7. Expected volume emission rates as a function of radial distance for meteoric Na excited by the Chapman oxidation-reduction cycle. The model uses parameters measured for the Diamond Ring meteor train.

from the all-sky Na imager. This is done in Plate 4. Plate 4(top) shows an image of the Diamond Ring taken by the camera. A precise calibration of the camera has not been done; so, for the purposes of the airglow intensity calculations, background Na emissions are assumed to be about 50 R, a typical value for the background Na airglow. The solid line plot in Plate 4(bottom) shows the background-subtracted emission intensity along the line shown cutting across the train in Plate 4(top). The dashed line plot in Plate 4(bottom) shows the calculated Na photon flux from the surface of the model train. The calculated profile is clearly much narrower than the observed profile. We believe that this is a consequence of the integrated response of the camera, each image from which represents a 90 s integration. An analysis of the winds affecting the Diamond Ring has been performed by *Grime et al.* [2000] and by *Drummond et al.* [this issue]. The horizontal winds were found to have a peak magnitude of around 70 m s^{-1}. Thus, after 90 s a portion of the train would have been expected to move ~6 km, in relatively good agreement with Plate 4.

The model also predicts more intense Na emissions than are observed. The predicted maximum intensity of ~20 R is about 4 times greater than the estimated observed maximum of 5 R. It should be pointed out that there are significant uncertainties involved in both the numerical model calculations and also in the imaged Na intensities presented here. Of particular importance to the Na emission calculations is the O_3 concentration since the Na airglow intensity is directly dependent on it. Observed O_3 concentrations over the 90-100 km height range of the Diamond Ring vary from about 1×10^7 to about 5×10^8 cm^{-3}. Since 1×10^8 cm^{-3} has been used in the modeling, the model may overestimate the emissions by an order of magnitude, or underestimate them by about a factor of 5. There is an additional uncertainty in the O_3 concentration due to the effects of meteor ablation. *Zinn et al.* [1999] predict depressed levels of O_3 in the atmosphere near the meteor resulting from dissociation by intense amounts of UV radiation emitted as the meteor traverses the atmosphere. This could obviously lead to reduced Na emissions, though it is unclear if this would have a significant effect after the first few minutes, when the trail has diffused outward enough to encounter fresh O_3. An additional source of uncertainty in the predicted Na emission levels results from the aforementioned uncertainty in α. If α is closer to 0.02, as indicated by *Hecht et al.* [2000], instead of 0.1 as is used here, then the predicted emissions would be reduced by a factor of 5, which would improve the agreement between the model and the observations. Larger values, up to about 0.6, have also been predicted for α, though such a large value seems unlikely and is not supported by experiment.

There is also significant uncertainty in the observed intensity levels, which are based on the assumption of a 50 R background emission. Background Na emissions are typically between about 20 and 200 R, and so, it might be expected that the observed Na intensity could be between about half and a few times what is shown in Figure 4. Thus, though it seems likely that the model overestimates somewhat the Na emissions, it should still be adequate for the purpose of the following analysis, which compares the predicted Na emissions to the total observed train luminosity.

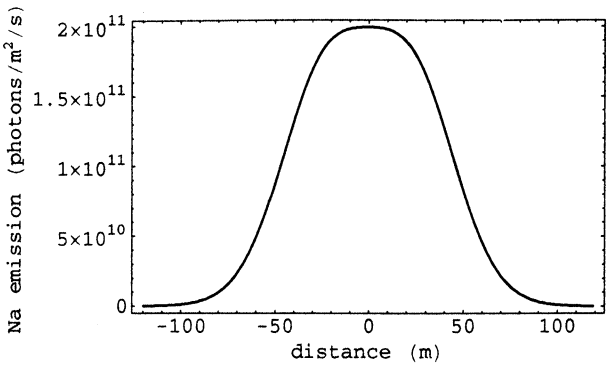

Figure 8. Predicted Na emissions along the train's width.

In section 3 the photometry of the Diamond Ring was investigated in some detail. Figure 4 shows the measured flux along several cuts across it. Peak emissions are between about 7 $\times 10^{13}$ and 22 $\times 10^{13}$ photons m^{-2} s^{-1} (7000-22,000 R), while the total emission per unit length of train, shown in Table 2, is between 2×10^{16} and 8×10^{16} photons m^{-1} s^{-1} (where the contributions from both emitting regions are added together for those regions where the train appears hollow). To compare these values with the expected Na emissions based on the numerical model, the Na photon surface emission rates at several points along the width of the train are calculated. This is done by correcting the radial volume emission intensity profile in Figure 7 for the proper viewing geometry of a ground-based observer. The result, shown in Figure 8, represents the predicted Na photon surface emission rate from the Diamond Ring meteor train, based on the measured Na density, diffusivity, and temperature. The model profile is much narrower than the observed train width at 82 s, which according to Figure 4 is nearly 400 m, even at its narrowest. Interestingly, though, the width does match fairly well that of the individual 'lines' for those parts of the train that appear as double. The width discrepancy could indicate that the value of the diffusivity used here is far too small. It seems more likely though that the train is initially much larger than the initial size of 1 m used here or that the train undergoes an initial rapid expansion, as described by *Jenniskens et al.* [2000c].

The peak Na emissions from the model are between 2 and 3 orders of magnitude less intense than the peak observed luminosity reported above. The total Na emission per unit length of the model train, obtained by integrating across the profile shown in Figure 8, was found to be 2×10^{13} photons m^{-1} s^{-1}, some 3 orders of magnitude smaller than the measured line emission from

the Photometrics CCD image. As was discussed above, the uncertainty in the modeled emission intensity is significant. However, since the comparison with the Na all-sky images of the Diamond Ring indicates that the model tends to overestimate the Na emissions, it is reasonable to conclude that Chapman's mechanism is capable of producing only a small portion of the observed persistent train luminosity. Hence we must search for alternative sources of enduring emissions.

4.1. Iron Oxide Emission

The spectroscopic observations obtained during the airborne campaign provide a partial answer. The visual emission is dominated by a a broad continuum emission that underlays the sodium D lines Figure 3. The measured integrated intensity of that continuum is about 40 times that of the sodium emission. Indeed, radiation from excited metal oxides produced as a result of the oxidation of meteoric metal atoms by O_3 in (18) has been suggested before as a source of train luminosity [*Baggaley*, 1976]. Iron is one of the more abundant meteoric metals, significantly more abundant than Na. FeO produced in the reaction of Fe with O_3 is known to produce radiation (primarily) in the FeO orange system [*West and Broida*, 1975] between 560 and 670 nm.

The previously described model is adjusted to include the presence of Fe, Mg, and Ca atoms. These are assumed to be present in typical chondritic proportions relative to Na as given by *Mason* [1971]. We note, however, that work published by *von Zahn et al.* [1999] indicates that Ca would not be expected to be present in its chondritic proportion in the trail. Since Ca is far less prevalent than Fe and Mg, though, this should not greatly affect the results. Table 3 shows the proportions used.

The following reactions are added to the model:

$$\mathrm{M} + \mathrm{O_3} \longrightarrow \mathrm{MO} + \mathrm{O_2} \tag{18}$$

$$\mathrm{MO} + \mathrm{O} \longrightarrow \mathrm{M} + \mathrm{O_2} \tag{19}$$

where M is taken to represent an Fe, Mg, or Ca atom. The rates for these reactions are taken to be $k_{18} = 3.5 \times 10^{-10} \exp(-146/T)$ cm^3 s^{-1} and $k_{19} = 3.0 \times 10^{-10}\sqrt{T/200}$ cm^3 s^{-1} [*Plane and Helmer*, 1994]. Using the Fe abundance given in Table 3, and assuming that 10% of FeO created radiates, the numerical model

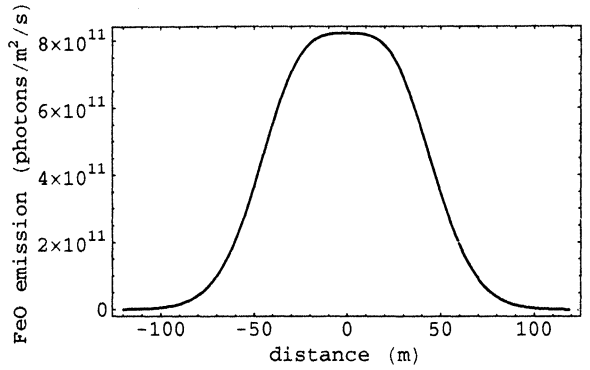

Figure 9. Predicted FeO orange band emissions along the train's width.

is used to estimate the expected FeO orange system intensity. Figure 9 shows the calculated FeO line emission intensity after the train has been allowed to evolve for 82 s. The emission peaks at about 8.0×10^{11} photons m^{-2} s^{-1} in the train center and is 4 times more intense than the Na emissions. Interestingly enough, this is a factor of 10 less than is observed. Even so, the FeO emission alone cannot account for the observed total luminosity in the CCD camera passband.

4.2. $O_2(b^1\Sigma_g^+)$ Emission

Other sources of emission will have to be found in the near-IR, between 700 nm and 1μ. Indeed, *Hapgood* [1980] observed significant intensity of persistent trains in this passband and the SOR near-IR all-sky camera detected persistent trains in the 750-900 nm OH airglow passband filter. Although there is some hint of OH emission in Figure 5, this emission is probably not from OH. OH airglow emissions are produced by the following reaction:

$$\mathrm{H} + \mathrm{O_3} \longrightarrow \mathrm{OH^*} + \mathrm{O_2}.$$

Since elevations in H or O_3 density are not expected in the wake of a meteor, there is no reason to expect an enhancement in OH emissions in even persistent trains. Hence we believe that the detected luminosity may not be due to OH but rather that the camera may have detected $O_2(b^1\Sigma_g^+)$ emissions similar to those reported by *Hapgood* [1980], except with the (0,1) component filtered out.

Table 3. Assumed Relative Abundances of Metallic Atoms in Meteor Trails

Element	Relative Abundance
Na	1.0
Fe	16.0
Mg	22.0
Ca	1.14

Table 4. Reaction enthalpies of interest and highest accessible vibrational state of $O_2(b^1\Sigma_g^+)$

Element	ΔH_{oxid} (eV)	ν	ΔH_{red} (eV)	ν
Na	1.54	-	2.50	5
Fe	3.17	9	0.87	-
Mg	2.39	3	1.60	-
Ca	2.87	7	1.20	-

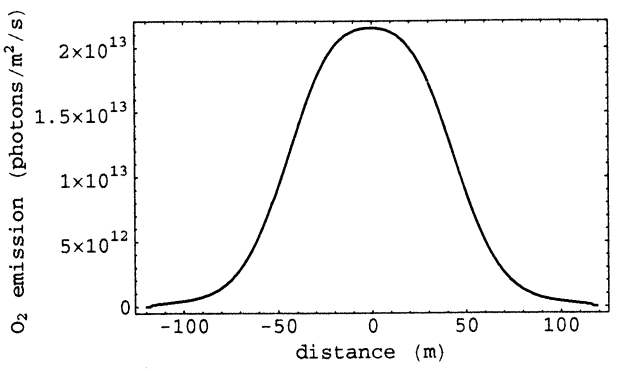

Figure 10. Predicted maximum emission of O_2.

Hapgood [1980] attributed the near-IR emission to the excitation of $O_2(b^1\Sigma_g^+)$ as a consequence of (5) of the Na cycle. That reaction is exothermic by 2.5 eV while the $b^1\Sigma_g^+$ state of O_2 lies 1.63 eV above the ground state, showing there is energy enough to produce the excited state and further vibrational excitation, up to the $\nu = 5$ state. This would lead to radiation in bands between about 540 nm and 1μ. Other meteoric metals, such as Fe, Mg, and Ca, undergo a similar sequence of oxidation-reduction reactions with atmospheric gases that could also lead to excited O_2. Table 4 shows the enthalpies of the oxidation and reduction reactions for Na, Mg, Fe, and Ca and the highest vibrational state of $O_2(b^1\Sigma_g^+)$ that could be excited in each reaction, assuming all of the excess energy of the reaction goes into excitation of O_2. It is clear that the oxidation by O_3 of Mg, Fe, and Ca is also sufficiently exothermic to excite $O_2(b^1\Sigma_g^+)$. Unfortunately, as is the case for Na, there seem to be no experimental measurements of how much $O_2(b^1\Sigma_g^+)$, if any, is produced in the process. We attempt here to calculate the maximum O_2 emissions that might be expected from our model meteor train.

Since we are interested in the maximum emission, we assume that (18) always produces an $O_2(b^1\Sigma_g^+)$ molecule and that reaction (5) does so when there is no excitation of the resulting Na atom. We further assume that all $O_2(b^1\Sigma_g^+)$ molecules that are not quenched produce detectable radiation. The transition from $b^1\Sigma_g^+$ to the $X^3\Sigma_g^-$ ground state is forbidden, and the radiative lifetime of the state is consequently very long ($\sim$12 s). Quenching of $O_2(b^1\Sigma_g^+)$ proceeds primarily via collisions with molecular nitrogen at a measured rate of $\sim 2 \times 10^{-15}$ cm^3 s^{-1} [*Hapgood*, 1980]. Adjustments to the model are made for the measured transition rate and for quenching.

Figure 10 shows the model results for the maximum $O_2(b^1\Sigma_g^+)$ surface emission after 82 s. The peak flux in Figure 10 is about 2.0×10^{13} photons m^{-2} s^{-1}, which is larger than the peak Na emission by more than 3 orders of magnitude. The integrated O_2 line emission was calculated to be $\sim 2.0 \times 10^{15}$ photons m^{-1} s^{-1}. Comparing with Figure 4, we see that the predicted peak O_2 emission is between about 0.1 and 0.3 of the measured peak emissions. Also, the integrated O_2 line emission is more than an order of magnitude weaker than what is measured.

It is possible that the $O_2(b^1\Sigma_g^+)$ emission is significantly larger than indicated in Figure 10, since only O_2 excited by reactions of meteoric metal species with atmospheric oxygen species has been included in the calculations. $O_2(b^1\Sigma_g^+)$ is also produced as a result of the recombination of oxygen atoms. Because it is likely that there are significantly elevated levels of O in the train, both from the meteor itself and from the dissociation of atmospheric molecules as predicted by *Zinn et al.* [1999], it is also likely that $O_2(b^1\Sigma_g^+)$ emissions from this source could be substantial.

Thus it seems that $O_2(b^1\Sigma_g^+)$ could potentially be a significant source of train luminosity. However, while it is possible that emissions from O_2 formed in meteor trains may be as strong as (or stronger than) is indicated in Figure 10, it is unclear what fraction of those emissions would be detectable by a ground-based observer. Atmospheric O_2 will absorb photons from transitions that terminate on the vibrational ground state, making them undetectable on the ground. Future efforts will, we hope, be made to answer this and other questions regarding this potentially important source of luminosity.

5. Role of Train Dynamics

Clues to the emission mechanisms are also provided by the unusual morphology and dynamical properties of the persistent trains, in particular by the double structure exhibited by a large portion of observed trains. As mentioned above, *Kelley et al.* [2000], *Chu et al.* [2000], and *Jenniskens et al.* [2000c] suggest that the chemical depletion of O_3 may be responsible. However, the luminosity decrease clearly visible in Figure 7, caused by such a chemical depletion, is not present in Figure 8, which represents more accurately the luminosity profile an observer would see. This is because contributions from the front and rear of the train appear to the ground-based observer, viewing the train from some distance, to be coming from its center, effectively filling (from the observer's point of view) the luminosity hollow there. Thus it appears that the chemical depletion of O_3 is insufficient to produce the double structure shown in Plate 3. *Zinn et al.* [1999] indicate that intense UV radiation from the strong shock wave that forms as the meteor traverses the atmosphere could lead to the dissociation of large amounts of O_3 and other molecules in the vicinity of the meteor trail. Perhaps such an additional O_3 sink could lead to a greater luminosity "hole" in the train's center. However, in addition to chemical depletion, *Jenniskens et al.* [2000c] included some O_3 dissociation in their analysis and found that the luminosity depletion thus created is still incapable of explaining the observations. The observed central luminosity is too large, even if there are no reactions

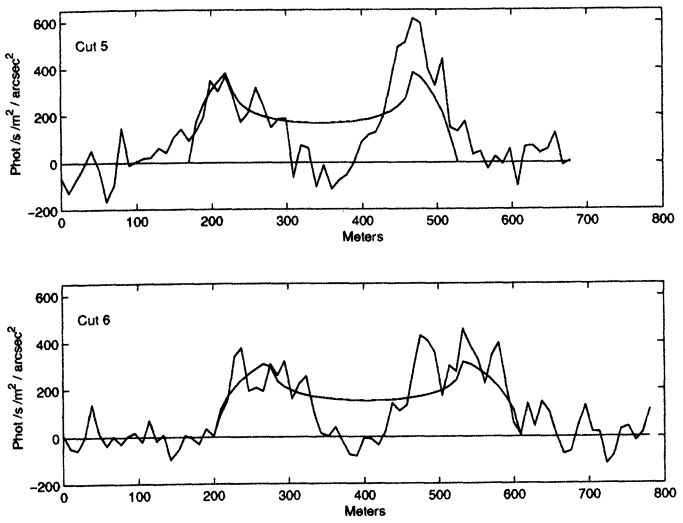

Figure 11. Expected luminosity profiles from a hollow cylinder and the actual profiles from cuts 5 and 6. Compare to the much better independent Gaussian fits of Figure 4.

in the center of the hollow tube. Figure 11 shows that poor fits result from assuming emission from only the walls of a cylinder and that the brightness is proportional to the path length through the tube. The size of the cylinder and the thickness of the walls are free parameters in the fit.

We examined the alternative possibility, that the two parallel beams of light in persistent trains are due to two trails rather than to the walls of a hollow cylinder. Indeed, the two parts of the observed train tend to have slightly different brightnesses [*Jenniskens et al.*, 2000c]. If we suppose that the emission areas arose independently, then at some points they might intertwine as they are blown into a loop by the winds. Videos over many minutes of this trail and others [*Drummond et al.*, 1999] show that the parallel trails do not ever twist, although the distance between them does vary slightly.

Yet another model that is suggested by combining the lidar data with our image is that two trails exist, but that above 96.5 km they are enshrouded in a broad region of emission, a fog. Not until the fog clears at lower altitudes do the parallel trails appear. The presence of a double peak in Figure 6 offers some proof of this. As shown in Figure 6, the lidar measured two peaks in Na density at an altitude just above 98 km. Whereas the lidar penetrated both, a clear image taken at the same time would have shown one trail behind the other. Our CCD image 43 s earlier is consistent with this model, showing only one small trail but superimposed on a larger fog at cut 2. Furthermore, the distance between the two trails measured by the lidar was $423 \sin(50) = 324$ m, comparable to the separations between the trails in cuts 3-6 of 245-380 m. At lower altitudes, where the trails are clearly parallel (cuts 3-6), the lidar would have only measured one of them since the beam was too narrow to be able to intercept both. This was probably the case for the lidar return at 92.2 km reported above and shown in Figure 2 and at the bottom of Figure 6, where only one trail was detected. The sizes of the trails measured by the lidar ($\sigma = 120$ and 61 m at 98 km altitude and 39 m at 92 km) are similar to the those measured from the CCD image (σ ranging from 34 to 68 m), as well as those of the model profiles in Figures 8-9. This lends further credence to this model.

Both models raise the question of why there are only two. If multiple fragments would lead to independent trails, then certainly, on occasion, there should be more than two side by side trails. Perhaps there is a segregation taking place, by mass, by composition, or even by charge. At any rate the dark central region of many of the trails we observed remains best explained as two independent trails, but further investigation is certainly required for an alternate or more complete explanation.

These alternative dynamic models do not help explain the observed missing luminous intensity. At best, they could add a factor of 2 to the integrated intensity. The answer to this question is rather an unidentified source of luminosity in the near-IR or an unidentified error in the luminosity calibrations.

6. Conclusions

The observations conducted at SOR during the peak of the 1998 Leonid meteor shower offered an excellent opportunity to study the phenomenon of persistent meteor trains. In particular, the lidar measurements of Na density, temperature, and diffusivity, coupled with the optical measurements from the various cameras and video cameras, made it possible for the first time to quantify the contribution of Na emissions to the persistent luminosity. The results reported here indicate that Na emissions can be expected to comprise only a very small fraction of the total observed (visible plus near-IR) intensity. Thus it seems that the *Chapman* [1955] mechanism cannot be the dominant source of enduring train luminosity. Furthermore, it seems that the chemical depletion of O_3 in the inner regions of the train near the axis is not sufficient to produce the hollow structure many persistent trains, including those discussed here, are reported to have. Indeed, the hollow structure remains most perplexing since Trowbridge's cylindrical shell model appears to be inadequate.

Metal oxides, in particular the FeO orange arc emission, contribute to the visible luminosity of trains, as indicated by the spectrum in Figure 3. We tentatively conclude that the persistent train luminosity is not totally accounted for, even by taking into account all the products of the metal oxidation-reduction reactions involving the recyclable metals.

Additional sources of luminosity likely exist in the 700-900 nm passband. We studied the emissions from

$O_2(b^1\Sigma_g^+)$, which occur in this wavelength range, and it may be excited by the oxidation-reduction chemistry of Na and other meteoric metals. The model results indicate that this has some promise, and the observation of enduring luminosity in the OH emission bandwidth, which we attribute to O_2, lends added credibility to this possibility. However, more work must be done before decisive conclusions can be drawn. Particularly useful would be experimental studies to measure the degree to which $O_2(b^1\Sigma_g^+)$ is excited by the relevant chemical reactions.

It should be noted that the model developed here is at the moment quite crude. Only the effects of particle diffusion and chemical kinetics are included. Perhaps more importantly, it is assumed that the background atmosphere remains undisturbed by the passage of the meteor. *Zinn et al.* [1999] is particularly interesting in this regard since they predict enormous levels of dissociation of O_3 and other molecules. Including such effects in future implementations could help explain many of the aspects of persistent trains.

Acknowledgments. We wish to thank the staff at Starfire Optical Range for their work in making this research possible. This research was funded under CEDAR grant ATM-9714736 from the Atmospheric Science Section of the National Science Foundation.

Janet G. Luhmann thanks the referees for their assistance in evaluating this paper.

References

Abe, S., N. Ebizuka, and J. Watanabe, Spectrum of meteor persistent train of 1998 Leonid, *Meteor. Planet. Sci., in press*, 2001.

Baggaley, W. J., Sodium emission from long enduring meteor trains, *Nature*, *257*, 567–568, 1975.

Baggaley, W. J., The role of the oxides of meteoric species as a source of meteor train luminosity, *Mon. Not. R. Astron. Soc.*, *174*, 617–620, 1976.

Baggaley, W. J., Meteor magnitudes and enduring trains, *Observatory*, *98*, 8–11, 1978.

Borovička, J., and P. Jenniskens, Time resolved spectroscopy of a Leonid fireball afterglow, *Earth Moon Planets*, *82-83*, 399–428, 2000.

Borovička, J., P. Zimnikoval, J. Škvarka, J. Rajchl, and P. Spurný, The identification of nebular lines in the spectra of meteor trains, *Astron. Astrophys.*, *306*, 995–998, 1996.

Chapman, S., Note on persistent meteor trails, in *The Airglow and the Aurora*, edited by E. B. Armstrong and A. Dalgarno, pp. 204–205, Pergamon, N.Y., 1955.

Chu, X., A. Z. Liu, G. Papen, C. S. Gardner, M. C. Kelley, J. D. Drummond, and R. Fugate, Lidar observations of elevated temperatures in bright chemiluminescent meteor trails during the 1998 Leonid shower, *Geophys. Res. Lett.*, *27*, 1815–1818, 2000.

Clemesha, B., D. Simonich, H. Takahashi, S. Melo, and J. Plane, Experimental evidence for photochemical control of the atmospheric sodium layer, *J. Geophys. Res.*, *100*, 18,909–18,916, 1995.

Drummond, J., M. C. Kelley, and C. S. Gardner, Leonid trails and lasers, a video presented at Asteroids, Comets, Meteors III, Cornell University, Ithaca, N.Y, July 26-30, 1999.

Drummond, J., C. S. Gardner, and M. C. Kelley, Catching a falling star, *Sky Tel.*, *99*, 46–49, 2000.

Drummond, J. D., B. W. Grime, C. S. Gardner, A. Z. Liu, X. Chu, and T. J. Kane, Observations of persistent Leonid meteor trails, 1, advection of the "Diamond Ring", *J. Geophys. Res.*, this issue.

Grime, B. W., T. J. Kane, A. Z. Liu, G. Papen, C. S. Gardner, M. C. Kelley, C. A. Kruschwitz, and J. D. Drummond, Meteor trail advection observed during the 1998 Leonid shower, *Geophys. Res. Lett.*, *27*, 1819–1822, 2000.

Hapgood, M. A., IR observation of a persistent meteor train, *Nature*, *286*, 582–583, 1980.

Hawkins, G. W., A hollow meteor train, *Sky Tel.*, pp. 168–169, 1957.

Hecht, J., S. Collins, C. Kruschwitz, M. Kelley, R. Roble, and R. Waltersheid, The excitation of the Na airglow from Coqui Dos rocket and ground based observations, *Geophys. Res. Lett.*, *27*, 453–456, 2000.

Jenniskens, P., S. Butow, and M. Fonda, The 1999 Leonid multi-instrument aircraft campaign–An early review, *Earth Moon Planets*, *82-83*, 1–26, 2000a.

Jenniskens, P., M. Lacey, B. Allan, D. Self, and J. Plane, FeO "orange arc" emission detected in optical spectrum of Leonid persistent train, *Earth Moon Planets*, *82-83*, 429–438, 2000b.

Jenniskens, P., D. Nugent, and J. Plane, The dynamical evolution a tubular Leonid persistent train, *Earth Moon Planets*, *82-83*, 471–488, 2000c.

Kelley, M. C., et al., First observations of long-lived meteor trains with resonance lidar and other optical instruments, *Geophys. Res. Lett.*, *27*, 1811–1814, 2000.

Kolb, C. E., and J. B. Elgin, Gas phase chemical kinetics of sodium in the upper atmosphere, *Nature*, *263*, 488–489, 1976.

Mason, B., *Handbook of Elemental Abundances in Meteorites*, Gordon and Breach, Newark, N.J., 1971.

Newton, H. A., Meteor trains, *Am. J. Sci. Arts*, *47*, 399–413, 1869.

Plane, J. M. C., and M. Helmer, Laboratory studies of the chemistry of meteoric metals, in *Research in Chemical Kinetics*, edited by R. G. Compton and G. Hancock, vol. 2, pp. 313–367, Elsevier Sci., New York, 1994.

Rajchl, J., J. Bocek, D. Ocenas, J. Skvarka, P. Zimnikoval, H. Murayama, and K. Ohtsuka, Results from several persistent train spectra intercompared, *Earth Moon Planets*, *68*, 479–486, 1995.

Trowbridge, C., The origin of luminous meteor trains, *Pop. Sci. Mon.*, pp. 402–407, 1911.

von Zahn, U., M. Gerding, J. Hoffner, W. McNeil, and E. Murad, Iron, calcium, and potassium atom densities in the trails of Leonids and other meteors: Strong evidence for differential ablation, *Meteor. Planet. Sci.*, *34*, 1017–1027, 1999.

West, J., and H. Broida, Chemiluminescence and photoluminescence of diatomic iron oxide, *J. Chem. Phys.*, *62*, 2566–2574, 1975.

Zinn, J., et al., Coordinated observations of two large Leonid meteor fireballs over northern New Mexico, and computer model comparisons, *Meteor. Planet. Sci.*, *34*, 1007–1015, 1999.

C. A. Kruschwitz, School of Electrical and Computer Engineering, Cornell University, 304 Rhodes Hall, Ithaca, NY 14853-3801 (e-mail: craigk@ee.cornell.edu)

M. C. Kelly, School of Electrical and computer engineering, Cornell University, 304 Rhodes Hall Ithaca, NY 14853-7501.

C. S. Gardner, Department of Electrical & Computer Engineering, University of Illinois, 2-114 Engineering Science Bldg., MC-266, 1101 West Springfield Avenue, Urbana, IL 61801 (cgardner@uiuc.edu)

G. R. Swenson, Department of Electrical and Computer Engineering, University of Illinois, 1308 West Main Street, 313 CSRL, Urbana, IL 61801, (swenson1@uiuc.edu)

A. Z. Liu, Department of Electrical and Computer Engineering, University of Illinois, 1308 West Main Street, 308 CSRL, Urbana, Illinois 61801, (liuzr@uiuc.edu)

X. Chu, Department of Electrical and Computer Engineering, University of Illinois, 1308 West Main Street, 308 CSRL, Urbana-Champaign, IL 61801, (xchu@uiuc.edu)

J. D. Drummond, Starfire Optical Range, Air Force Research Laboratory, 3550 Aberdeen Avenue, SE, Kirtland AFB, NM 87117-5776, (jack.drummond@kirtland.af.mil)

B. W. Grime, Air Force Research Laboratory, 3550 Aberdeen Avenue SE, Kirtland AFB, New Mexico 87117-5776,

W. T. Armstrong, Los Alamos National Laboratory, EES-8, MS-F659, Los Alamos, NM 87545, (wta@lanl.gov)

J. M. C. Plane, School of Environmental Sciences, University of East Anglia, Bluebell Road, Norwich, NR4 7TJ (J.Plane@uea.ac.uk)

P. Jenniskens, The SETI Institute, NASA Ames Research Center, Mail Stop 239-4, Moffett Field, CA 94035-1000 9peter@max.arc.nasa.gov0

(Received May16, 2000: revised March 5,200:
accepted March 16,2001)